European Radiology (2019) 29:4624–4634
https://doi.org/10.1007/s00330-019-6005-6

COMPUTED TOMOGRAPHY

DXA-equivalent quantification of bone mineral density using dual-layer spectral CT scout scans

Alexis Laugerette[1,2] · Benedikt J. Schwaiger[1] · Kevin Brown[3] · Lena C. Frerking[4] · Felix K. Kopp[1] · Kai Mei[1] · Thorsten Sellerer[2] · Jan Kirschke[5] · Thomas Baum[5] · Alexandra S. Gersing[1] · Daniela Pfeiffer[1] · Alexander A. Fingerle[1] · Ernst J. Rummeny[1] · Roland Proksa[4] · Peter B. Noël[1,6] · Franz Pfeiffer[1,2]

Received: 31 August 2018 / Revised: 6 December 2018 / Accepted: 11 January 2019 / Published online: 13 February 2019

Abstract

Objectives To develop and evaluate a method for areal bone mineral density (aBMD) measurement based on dual-layer spectral CT scout scans.

Methods A post-processing algorithm using a pair of 2D virtual mono-energetic scout images (VMSIs) was established in order to semi-automatically compute the aBMD at the spine similarly to DXA, using manual soft tissue segmentation, semi-automatic segmentation for the vertebrae, and automatic segmentation for the background. The method was assessed based on repetitive measurements of the standardized European Spine Phantom (ESP) using the standard scout scan tube current (30 mA) and other tube currents (10 to 200 mA), as well as using fat-equivalent extension rings simulating different patient habitus, and was compared to dual-energy X-ray absorptiometry (DXA). Moreover, the feasibility of the method was assessed in vivo in female patients.

Results Derived from standard scout scans, aBMD values measured with the proposed method significantly correlated with DXA measurements ($r = 0.9925$, $p < 0.001$), and mean accuracy (DXA, 4.12%; scout, 1.60%) and precision (DXA, 2.64%; scout, 2.03%) were comparable between the two methods. Moreover, aBMD values assessed at different tube currents did not differ significantly ($p \geq 0.20$ for all), suggesting that the presented method could be applied to scout scans with different settings. Finally, data derived from sample patients were concordant with BMD values from a reference age-matched population.

Conclusions Based on dual-layer spectral scout scans, aBMD measurements were fast and reliable and significantly correlated with the according DXA measurements in phantoms. Considering the number of CT acquisitions performed worldwide, this method could allow truly opportunistic osteoporosis screening.

Key Points

- *2D scout scans (localizer radiographs) from a dual-layer spectral CT scanner, which are mandatory parts of a CT examination, can be used to automatically determine areal bone mineral density (aBMD) at the spine.*

Summary statement The presented method, based on spectral CT scout scans, allows to reliably determine areal BMD in state-of-the-art phantom and in sample patient data. The results suggest that the performance of the method is possibly similar to that of DXA for the phantom experiments performed in this work.

Electronic supplementary material The online version of this article (https://doi.org/10.1007/s00330-019-6005-6) contains supplementary material, which is available to authorized users.

✉ Peter B. Noël
peter.noel@uphs.upenn.edu

[1] Department of Diagnostic and Interventional Radiology, Klinikum rechts der Isar, Technical University of Munich, Ismaninger Str 22, 81675 Munich, Germany

[2] Biomedical Physics & Munich School of BioEngineering, Technical University of Munich, Garching, Germany

[3] Philips Healthcare, Cleveland, OH, USA

[4] Philips Research Laboratories, Hamburg, Germany

[5] Section of Diagnostic and Interventional Neuroradiology, Technical University of Munich, Munich, Germany

[6] Department of Radiology, Perelman School of Medicine, University of Pennsylvania, Philadelphia, PA, USA

• *The presented method allowed fast (< 25 s/patient), semi-automatic, and reliable DXA-equivalent aBMD measurements for state-of-the-art DXA phantoms at different tube settings and for various patient habitus, as well as for sample patients.*

• *Considering the number of CT scout scan acquisitions performed worldwide on a daily basis, the presented technique could enable truly opportunistic osteoporosis screening with DXA-equivalent metrics, without involving higher radiation exposure since it only processes existing data that is acquired during each CT scan.*

Keywords Multidetector computed tomography · Dual-energy X-ray absorptiometry · Bone density · Osteoporosis · Spine

Abbreviations

ANCOVA	Analysis of covariance (a statistical analysis technique)
AP	Antero-posterior
BMC	Bone mineral content (g)
BMD	Bone mineral density (mg/mL), sometimes also used for areal bone mineral density (aBMD, g/cm^2)
CV	Coefficient of variation
DXA, DEXA	Dual-energy X-ray absorptiometry
ESP	European Spine Phantom
HA	Calcium-hydroxyapatite, the main mineral component of bone
IV	Intravenous (contrast agent)
QCT	Quantitative computed tomography
VMSI	Virtual mono-energetic scout image

Introduction

It is estimated that 28 million individuals are affected by osteoporosis in the European Union alone, with increasing prevalence due to the aging population [1, 2].

Numerous clinically accepted methods exist to determine bone mineral density (BMD). Dual-energy X-ray absorptiometry (DXA) is considered the gold standard [3]. Whereas this technique provides relatively fast and low-dose acquisitions, up to 70% of eligible women and significantly more men do not undergo BMD screening at least once in their lives [4], and subsequently, only 10–22% of patients receive adequate therapy [2]. Moreover, DXA suffers from limitations, such as its susceptibility to bone size and its sensitivity to degenerative changes [5]. Therefore, DXA is very often used to confirm an already suspected osteoporotic status. Quantitative CT (QCT), on the other hand, is a fast and accurate method [6] to identify patients with osteoporosis; however, radiation doses and cost are considerably higher than those for DXA, limiting its use [7]. Therefore, several methods for assessing BMD are currently being investigated, such as using asynchronously calibrated MDCT examinations or even low-dose PET/CT examinations [8].

A mandatory part of CT examinations are scout scans, which are essentially acquired in order to ensure correct patient positioning. The CT scout scan thus exposes patients to radiation doses without providing relevant diagnostic information. It has been demonstrated previously that the CT scout scan can significantly contribute to the integral dose of a full examination [9–11]. Therefore, it would be highly beneficial if imaging data obtained from scout scans could be used for opportunistic BMD analyses. Dual-energy CT (DECT) systems may provide this opportunity: DECT allows to decompose the low- and high-energy data into a pair of components corresponding to the physical effects responsible for the observed image (i.e., the photo-electric effect and Compton scattering in the X-ray energy range used for diagnostic imaging). This modified pair of images can be combined together to produce so-called virtual mono-energetic images [12], which can then be used to retrieve aBMD.

Recent studies assessed BMD determination based on DECT [13, 14]. However, the methods used volumetric (3D) CT data, which could suffer in an opportunistic screening situation from the presence of IV contrast agent. Two-dimensional (2D) scout scan images, when acquired with a dual-layer spectral CT scanner, could be used to compute the BMD, similar to DXA, since they are acquired simultaneously and thus perfectly registered [15–17].

The purpose of this study was to develop a fast, semi-automatic, low-dose, spectral CT scout scan-based method to determine the areal BMD (aBMD) and enable eventually an early-stage, truly opportunistic BMD screening. The feasibility of the method was assessed with a standardized BMD phantom and patient data.

Materials and methods

BMD quantification based on spectral CT scout scans

An algorithm utilizing spectral CT scout scan raw data was developed in order to compute aBMD at the spine (vertebrae L1-L4) semi-automatically. The scout scan raw data of the spectral CT scanner (IQon spectral CT, Philips Healthcare) corresponds to two perfectly registered frontal projection images generated from the low- and high-energy detector layers. The developed algorithm, mimicking the principle of standard DXA, comprises different steps, which are mainly preprocessing of the raw data and conversion to a pair of photo-

electric and scatter scout images, segmentation (vertebrae, soft tissue, background), and computation of aBMD. A detailed overview of the developed algorithm for BMD quantification can be found in the supplemental material. On a standard PC equipped with a modern processor and no GPU, the total segmentation time (including user interactions and display of segmentation results) was about 20 s. The computation and display of BMD results was then achieved in less than 1 s. This process could be further optimized to obtain much higher performance.

Experimental evaluation

Dual-layer spectral CT

Both the phantom measurements and patient examinations were acquired with a dual-layer spectral CT [17, 18]. The unmodified clinical routine protocols were applied, with a tube current of 30 mA and a peak voltage of 120 kVp, unless otherwise specified. Figure 1 (upper row) illustrates the dual-layer spectral CT scanner used.

DXA

DXA measurements were performed the way they are obtained in clinical routine at our institution, on a standard DXA device, with a standard protocol (GE Lunar Prodigy, GE Healthcare). DXA images were automatically analyzed and reports were generated with a vendor-specific software (Lunar Prodigy enCORE, version 15, GE Healthcare).

Phantoms

A standard phantom for quality assurance in DXA and QCT was examined for this study (ESP, European Spine Phantom, QRM). The phantom was extensively studied by Kalender et al [19] and allows to check reproducibility and accuracy for the following quantities: aBMD (g/cm^2) and BMC (g) in DXA, trabecular and cortical bone mineral density in QCT (mg/mL), and cortical thickness in QCT. The phantom contains three internal lumbar vertebra inserts composed of varying amounts of calcium-hydroxyapatite (HA), covering the full physiological range of BMD values. The size, HA concentration, and expected DXA BMD (AP) value of the inserts are precisely tabulated by the manufacturer (see Table 1). The entire ESP has an oval shape with flattened sides and the dimensions of a typical patient abdomen ($260 \times 180 \times 110$ mm^3). Inserts are embedded in a water-equivalent plastic. For one series of experiments, the ESP was consecutively placed in two fat-equivalent extension rings, in order to simulate different degrees of obesity (extension rings M and L, QRM). Figure 1 (lower row) illustrates the ESP accompanied by the extension rings.

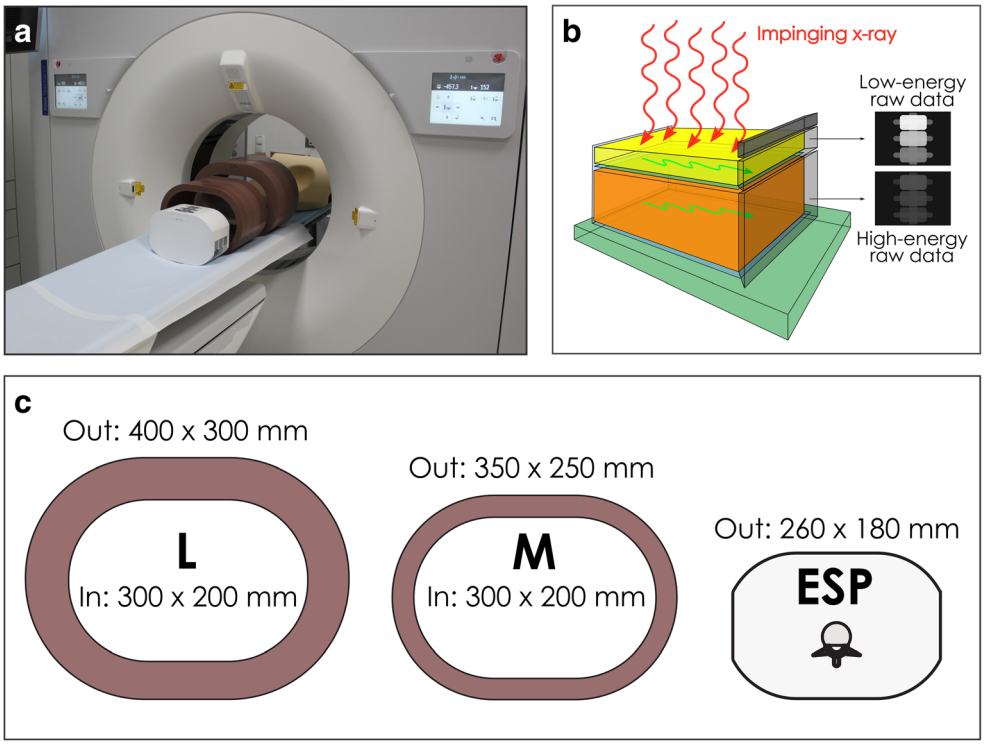

Fig. 1 Dual-layer spectral CT scanner and phantoms used in this study. (**a**) Setup for phantom measurements with the European Spine Phantom (ESP) and the two fat extension rings in a dual-layer spectral CT scanner. (**b**) Working principle of a dual-layer detector: an X-ray beam impinges on a dual-layer detector pixel, and the low-energy photons are absorbed in the top scintillator, while the high-energy photons are absorbed in the bottom scintillator. Visible light is generated and directed to side-looking photodiode arrays which enable the acquisition of the low- and high-energy raw data. (**c**) Dimensions of the ESP and fat extension rings, which can be placed around the phantom

Table 1 Properties of interest of the European Spine Phantom used for this study. Errors are given by the manufacturer

	L1	L2	L3
Soft tissue (bulk) material	Water-equivalent plastic		
Spongious bone mineral density (mg/mL) for QCT	50 ± 1.5 HA	100 ± 3 HA	200 ± 6 HA
Areal bone mineral density (g/cm^2) for DXA (AP)	0.500 ± 0.015	1.000 ± 0.030	1.500 ± 0.045

Experiments performed with the ESP

For each series of scans acquired using the ESP, as presented below, only the scout scan was acquired and exported, and no volumetric data was obtained.

Comparison of the scout scan-based method (at 30 mA) to DXA

In order to assess the accuracy and precision of the developed method, the ESP was repeatedly scanned (20 times) with the spectral CT at 30-mA tube current, on the same day, repositioning the phantom after each scan. To allow a fair comparison between the developed method and DXA, the ESP was also scanned 20 times with the DXA device, with the standard protocol, again repositioning the phantom after each scan.

Applicability of the method at different tube currents

ESP scout scans were acquired with a spectral CT at eight different tube currents (10, 20, 30, 50, 70, 100, 150, and 200 mA), with four repetitions for each tube current, without repositioning the ESP, to assess the applicability of the method on a large tube current range. The analysis of each scan in this series was repeated twice; consequently eight data points were available for each tube current and for each ESP insert. For comparison purposes, the ESP was scanned eight times with the DXA device, using the standard protocol, without repositioning the phantom.

Applicability of the method to different patient sizes

Since one challenge of osteoporosis diagnostics is that DXA measurements can be influenced by the habitus of the patient [20], a series of scout scans was acquired using three different tube currents (30, 50, and 150 mA) on the ESP, which was surrounded by two different fat extension rings, simulating different degrees of obesity and thus allowing to study the applicability of the developed method for different patient habitus. Each scout scan was performed four times and the analysis was repeated twice. The same phantom configurations were each scanned eight times with the DXA device using the standard protocol in order to compare the performance of the developed CT scout scan-based method with the state-of-the-art DXA for different degrees of obesity of the patients.

In vivo aBMD estimation

In order to assess the applicability of the developed method in patient datasets, two patients, with available dual-energy scout scan raw data and without prior application of oral contrast agent, were retrospectively selected. A 22-year-old female patient scanned with a kidney stone low-dose protocol and a 77-year-old female patient scanned with a routine thorax/abdomen protocol were selected. Both patients had no conditions affecting bone metabolism other than postmenopausal osteoporosis in the latter case. Institutional review board approval was obtained prior to this study (Ethics Committee, Technische Universität München, München, Germany), and all analyses were performed in accordance with relevant institutional and legislative guidelines and regulations. Written informed consent was waived for this retrospective analysis of routinely acquired imaging data. Both scans were performed at the routine tube current of 30 mA, and the images were analyzed using the method described above. The results obtained for these patients were compared to age-adapted reference BMD values for Caucasian women [21].

Statistical analysis for phantom experiments

Statistical analysis was performed with MATLAB R2017a (The MathWorks Inc.), with $p < 0.05$ indicating significant differences, unless otherwise specified.

To assess the short-term precision of the proposed scout scan-based method and of DXA, i.e., the reproducibility of the diagnostic techniques, coefficients of variation (CV (%)) were computed for both techniques and defined as the ratio of standard deviation to mean measured BMD at each ESP insert. To assess their accuracy, i.e., the degree to which the measured values deviate from the true values, relative errors were computed with respect to the ESP specifications provided by the manufacturer. Ninety-five percent confidence intervals for the three inserts of the ESP were calculated for both methods to allow for comparison.

To show correlations between DXA and the proposed scout scan-based technique, Pearson's correlation coefficients were calculated. In order to demonstrate the agreement between the two techniques, linear regression models of the measured BMD and the nominal BMD were computed both for the developed method and for DXA, and analysis of covariance (ANCOVA) was applied to assess for the similarities between the slopes obtained through these regression lines, i.e., to

explain the measured BMD (quantitative variable) with the nominal BMD (quantitative explanatory variable) and the measurement method, e.g., scout scan-based method or DXA (qualitative explanatory variable). The same approach was used to study the applicability of the scout scan-based method when using different tube currents.

To study the applicability of the proposed technique in patients with different degrees of obesity, Bland-Altman plots were computed with respect to the measurements assessed using the DXA device, for the three phantom configurations studied, i.e., the ESP without extension ring, the ESP placed in a small extension ring (M) and in a big extension ring (L). Since all experiments were performed with the ESP, containing three vertebral inserts, the presented statistical analysis should be considered with caution, within the limits of these three available measurable BMD values.

Results

Comparison of the scout scan-based method (at 30 mA) to DXA

The obtained relative errors (ε), coefficients of variation (CV), and 95% confidence intervals, computed for the scout scan-based method and for DXA, are presented in Table 2. The obtained values show that the developed method is performing either as well as the DXA regarding accuracy (ε) and precision (CV), or even better in comparison with the DXA, especially for low BMD values (accuracy DXA, 8.3%; scout, 4.79%). The mean accuracy was 4.12% for DXA and 1.60% for the proposed method. The mean precision was 2.64% for DXA and 2.03% for the CT scout scan-based method. From the worst coefficient of variation for both methods, a least significant change (LSC) was extracted [22] and was found to be 9.4% for DXA and 10.0% for the proposed method, demonstrating that both methods are performing relatively similarly. The correlation coefficient was computed between the datasets ($r = 0.9925$, $p < 0.001$) and confirmed the similarity observed in the linearity plot (Fig. 2). Moreover, ANCOVA demonstrated no strong evidence toward different slopes (slope_DXA = 0.9494; slope_scout = 0.9754) between the two methods ($p = 0.0623$, $R^2 = 0.994$), suggesting a relatively good agreement between both methods.

Applicability of the method using different tube currents

Linear regressions were computed at each tube current for the scout scan-based method, and linearity plots were compared to DXA, similarly as the experiment described in the previous section (Fig. 3). First of all, it should be noticed that the displayed errors were overall smaller than those in the previous case, since the ESP was kept at a fixed position for these measurements. For all analyzed tube currents, the linear regressions were found to be relatively similar to the original 30-mA case presented in the previous section. This was confirmed by ANCOVA since no slopes were found to be significantly different from the original 30-mA case ($0.2043 < p < 0.9999$). These results would suggest that the proposed method is applicable on a large range of tube parameters, which could be useful for the application of the technique in obese patients.

Applicability of the method to different patient sizes

Figure 4 presents three Bland-Altman plots obtained for the ESP respectively surrounded by no fat ring (Fig. 4a), by a small fat ring M (Fig. 4b), and by a large fat ring L (Fig. 4c). The plots were obtained by computing the mean and the differences in measured BMD between DXA and the developed spectral CT scout scan-based method, for each of the three inserts of the ESP, and in four repeated measurements. On the ESP without fat surrounding (Fig. 4a), it was observed that the CT scout scan-based method gave similar results in comparison with the reference DXA measurements throughout all measured currents. However, when the phantom was larger, as shown in the two other plots (Fig. 4b, c), the results obtained by the proposed technique were less accurate, especially if the tube current was not sufficiently high. As shown in the plots, a sufficiently high current, like 150 mA, gave reliable results, even for the largest phantom configuration, and still allowed BMD estimation.

In vivo aBMD estimation

The segmentation results of the developed algorithm are illustrated in Fig. 5 for the two selected female patients. aBMD values computed for these patients with the developed method are presented in Table 3. The obtained BMD values were concordant with expected BMD values in age-matched women taken from the literature [21]. Moreover, the obtained BMD values were significantly different ($p = 0.0173$) from each other.

Discussion

In this study, it was demonstrated based on extensive phantom measurements that DXA-equivalent BMD estimation is feasible with 2D scout scans acquired using a dual-layer spectral CT scanner. The developed method showed a substantial agreement with DXA, which is considered to be the gold standard for BMD measurements. The evaluation was performed using a state-of-the-art phantom for quality control

Table 2 Relative errors (accuracy), coefficients of variation (short-term precision), and 95% confidence intervals measured on the ESP for DXA and for the developed CT scout scan-based method. The phantom was repositioned between each one of the 20 scans performed

	Accuracy relative errors (%)			Short-term precision CV (%)			95% confidence intervals		
	L1	L2	L3	L1	L2	L3	L1	L2	L3
DXA	8.30	4.66	− 0.60	1.99	2.53	3.39	[0.52; 0.56]	[0.99; 1.10]	[1.39; 1.59]
Localizer-based method (30 mA)	4.79	0.04	− 0.04	1.24	3.63	1.22	[0.51; 0.54]	[0.93; 1.07]	[1.46; 1.53]

and performance evaluation of DXA devices. The proposed method exhibits similar accuracy and precision as DXA, and even better than DXA for low BMD values, which could be of particular interest in the context of osteoporosis screening. However, this could be due to differences in the segmentation techniques used for both measurements. It has to be noted that the values obtained for accuracy and precision of DXA are slightly higher than usual, since the phantom was voluntarily repositioned with some errors. This was performed in order to simulate the suboptimal patient positioning that could be encountered with the CT scout scan-based method and thus to facilitate comparability of both methods in identical conditions. Indeed, padded boxes are used in DXA examinations in order to flatten the spine and generally to minimize imaging artifacts, which might not be feasible with the scout scan-based method considering the clinical workflow and the scanner geometry. Moreover, it has to be acknowledged that the presented scout scan-based BMD estimation method, because it is based on 2D images, would suffer from exactly the same artifacts and errors as DXA, such as dependency of the estimated BMD on bone size, overlaying soft tissue or the presence of aortic calcifications. In particular, the method may only be applicable to patients without oral contrast agent, similarly to DXA.

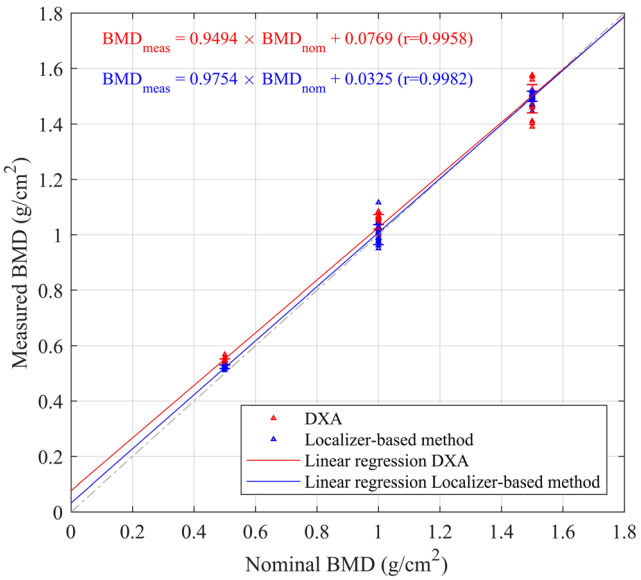

Fig. 2 Linearity plot showing similarity of the linear regressions obtained for DXA and the localizer-based method at 30 mA for measurement on the ESP. Nominal BMD values were provided by the manufacturer of the ESP. Error bars indicate ± one standard deviation. The gray dashed line represents the first diagonal (target line)

Limitations of the proposed method regarding the dependency on patient size were investigated by scanning thicker phantom configurations. At low tube currents, the BMD determination was less accurate in larger phantoms than in thinner phantoms, simulating different degrees of obesity. This could be explained by the decreased image quality observed at low currents (lose dose) for larger patients, which is due to very low photon counts reaching the X-ray detector. A further limitation of our study, which also affects the dose efficiency as well as patient sizes, was a decision to acquire data only with a tube voltage of 120 kVp. We could illustrate, in this initial study, that the concept works with 120 kVp, but technically an aBMD measurement should be a possibility with different tube settings. One example would be to utilize low tube voltage for smaller patients. However, reliable and robust results can be achieved for different patient habitus, if the tube current is adapted to individual patient sizes. For phantom measurements, it has to be noted that no power analysis was performed previously, since this study is a feasibility study concerning a method that has not been reported before. Moreover, for the phantom employed in this study, a calibration for areal BMD values was not available, but for volumetric BMD values, showing minor deviations from the nominal values within ± 1.6%. Therefore, the accuracy values presented in this work must be considered as general indicators for the performance of the described method.

Finally, it was shown that the CT scout scan-based BMD estimation also gives plausible results when applied to data from two patients, showing the feasibility and applicability of the method using patient data. BMD values computed for a 22-year-old female patient and a 77-year-old female patient were significantly different and showed good agreement with

Fig. 3 Linearity plots obtained for different tube currents with the proposed spectral CT scout scan-based method, compared to DXA. The red DXA regression line is the same in all plots and is given for comparison and visualization purposes. Slopes of the linear regressions for the scout scan-based technique are in all cases not significantly different from the original 30-mA regression line slope. The gray dashed lines represent the first diagonal (target lines)

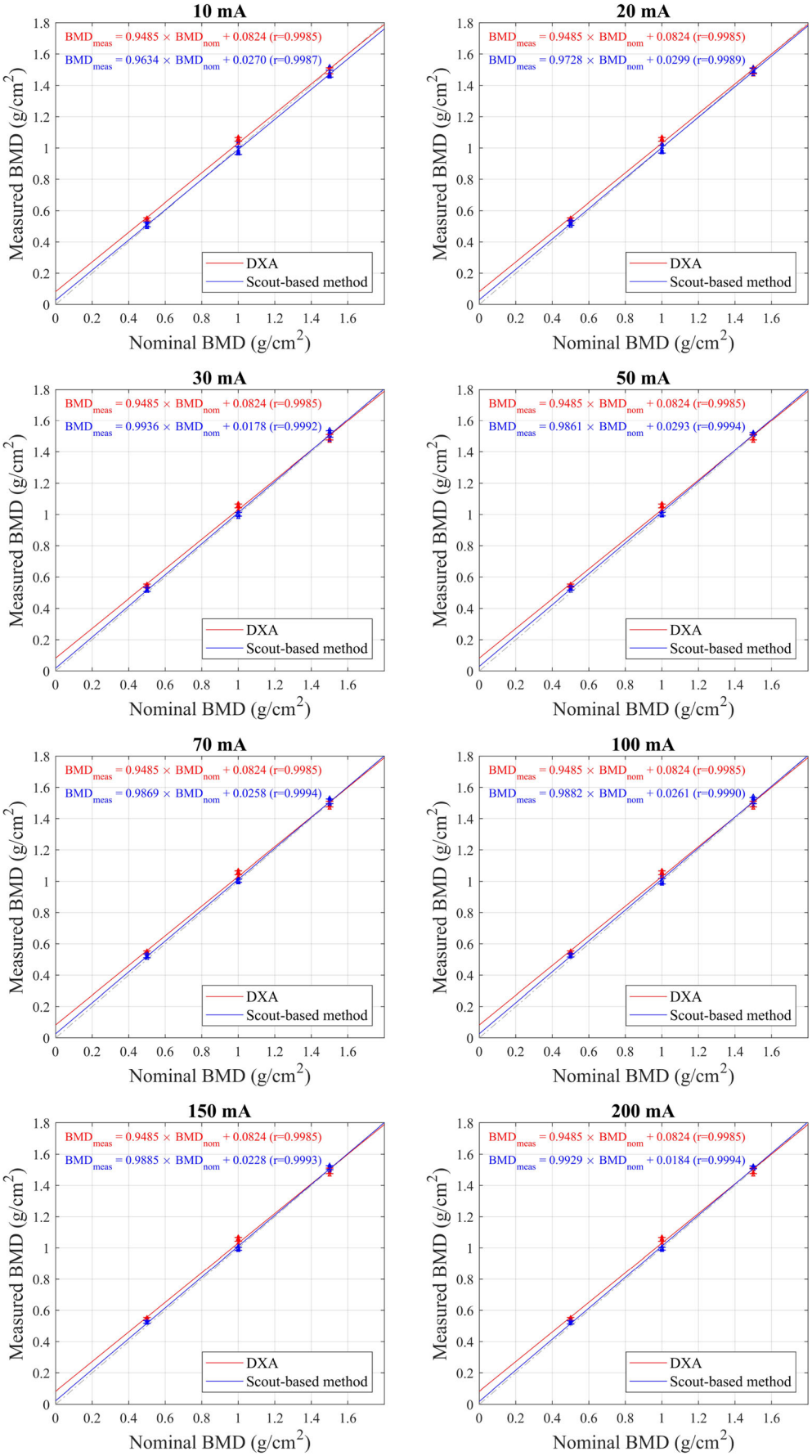
10 mA
BMD_meas = 0.9485 × BMD_nom + 0.0824 (r=0.9985)
BMD_meas = 0.9634 × BMD_nom + 0.0270 (r=0.9987)
20 mA
BMD_meas = 0.9485 × BMD_nom + 0.0824 (r=0.9985)
BMD_meas = 0.9728 × BMD_nom + 0.0299 (r=0.9989)
30 mA
BMD_meas = 0.9485 × BMD_nom + 0.0824 (r=0.9985)
BMD_meas = 0.9936 × BMD_nom + 0.0178 (r=0.9992)
50 mA
BMD_meas = 0.9485 × BMD_nom + 0.0824 (r=0.9985)
BMD_meas = 0.9861 × BMD_nom + 0.0293 (r=0.9994)
70 mA
BMD_meas = 0.9485 × BMD_nom + 0.0824 (r=0.9985)
BMD_meas = 0.9869 × BMD_nom + 0.0258 (r=0.9994)
100 mA
BMD_meas = 0.9485 × BMD_nom + 0.0824 (r=0.9985)
BMD_meas = 0.9882 × BMD_nom + 0.0261 (r=0.9990)
150 mA
BMD_meas = 0.9485 × BMD_nom + 0.0824 (r=0.9985)
BMD_meas = 0.9885 × BMD_nom + 0.0228 (r=0.9993)
200 mA
BMD_meas = 0.9485 × BMD_nom + 0.0824 (r=0.9985)
BMD_meas = 0.9929 × BMD_nom + 0.0184 (r=0.9994)
DXA
Scout-based method
Measured BMD (g/cm²)
Nominal BMD (g/cm²)

age-matched reference BMD values for Caucasian women, suggesting that the developed method could be well suited for routine clinical cases. Unfortunately, corresponding DXA BMD values for these patients were not available, since the regulation at our institution does not allow additional scans for patients when they are for research purposes only. Therefore, the presented patient results should be considered as an initial feasibility indicator, but with caution, as they do not represent any statistically validated finding since they are based on two patients only.

Other commercially available methods were suggested to provide opportunistic BMD screening, like a BMD software (CliniQCT, Mindways) which does not require any calibration phantom. This method estimates an aBMD which is cross-calibrated to the NHANES dataset in addition to providing volumetric BMD results. However, like other volumetric BMD testing techniques, these methods remain based on 3D datasets, which can potentially not cover the abdomen and could suffer from potential intravenous contrast agent application, and they are still not standard examinations.

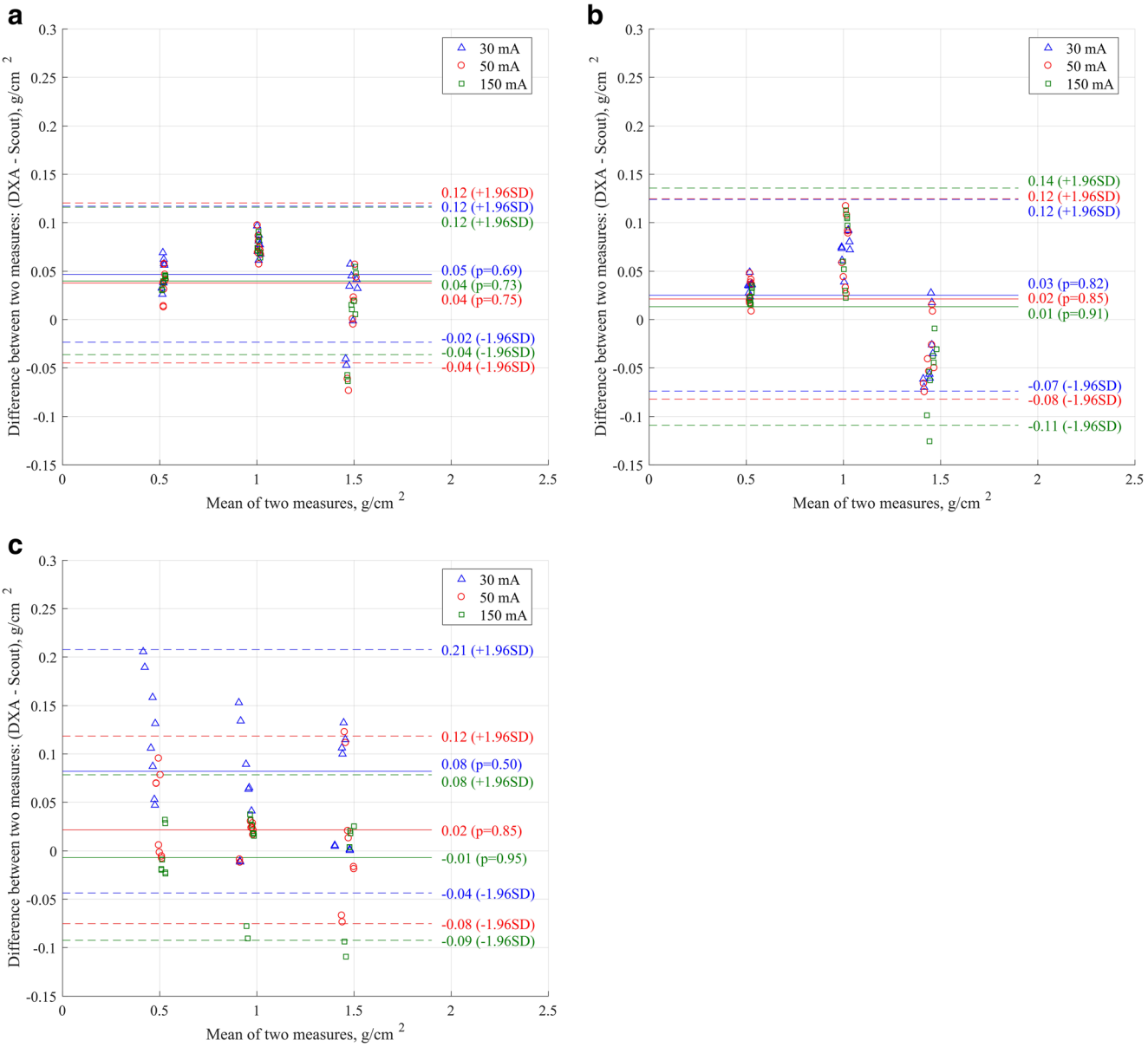

Fig. 4 Bland-Altman plots obtained by comparing the developed scout-based method at different tube currents with standard DXA, measuring different configurations of the ESP phantom. The plots respectively correspond to the ESP without any surrounding extension ring (**a**), the ESP placed in a small fat extension ring (**b**), and the ESP placed in a large fat extension ring simulating a higher degree of obesity (**c**). For larger phantoms (**c**), the low-current variants are not as accurate as with thin phantoms, demonstrating the limits of the proposed method when the patient is too large to allow a sufficiently good scout image quality and thus, enable BMD determination. A higher tube current could overcome this problem, as shown in (**c**)

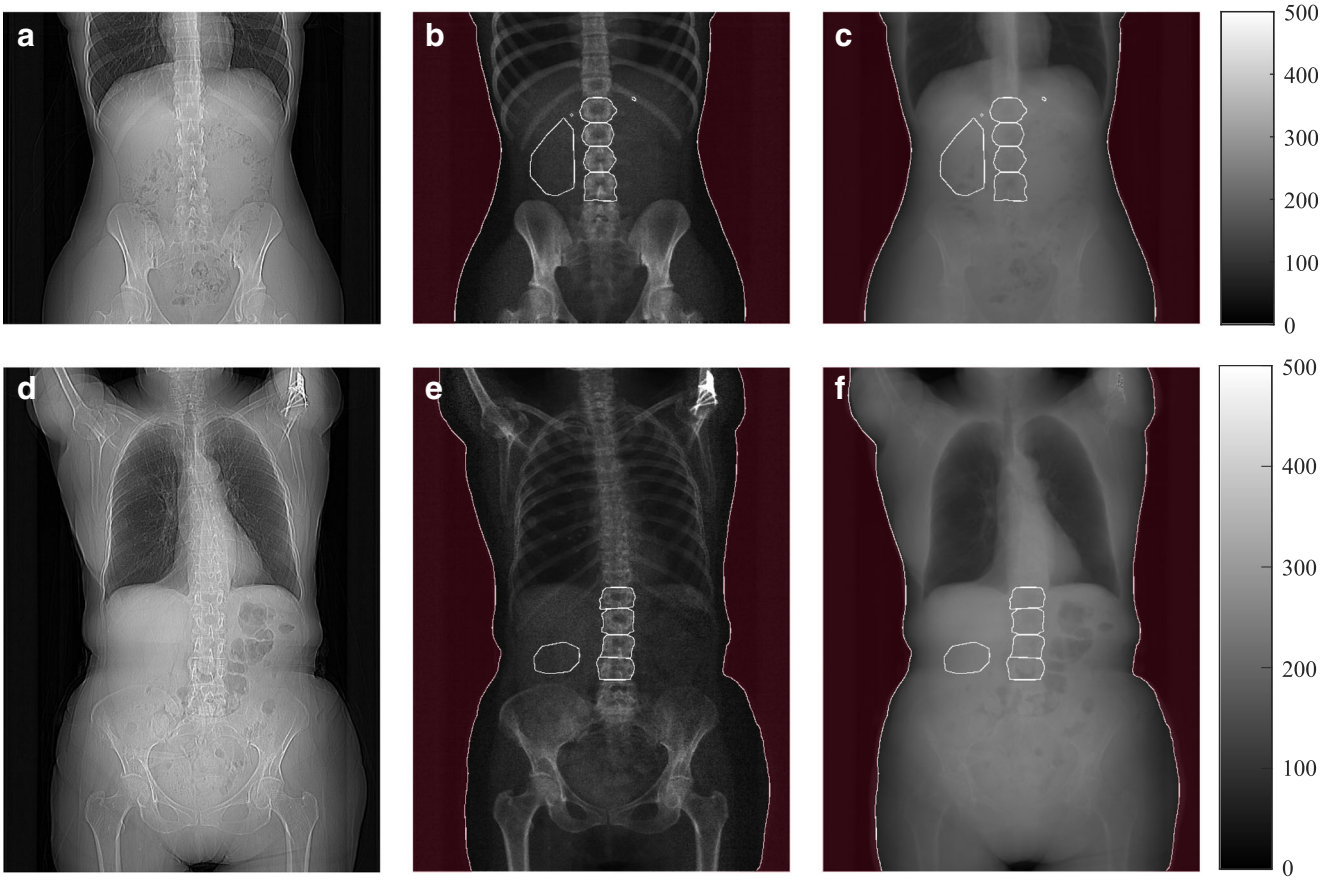

Fig. 5 Comparison of conventional scout image (**a**, **d**) with the photo-electric (**b**, **e**) and Compton (**c**, **f**) scout images, showing the good separation of bones and soft tissue allowing for simple segmentation and effective determination of BMD. The images are shown for a 22-year-old female patient (top, **a**–**c**) and for a 77-year-old female patient (bottom, **d**–**f**). The segmented areas are delineated with white lines corresponding to the extracted masks and are respectively background (dark red overlay), pure soft tissue region in the abdomen, and the four vertebrae L1 to L4 (from top to bottom). Units for the photo-electric and Compton scout images are equivalent path length (mm) in virtual objects having photo-electric-like or Compton-like attenuation coefficients

Nevertheless, it should be acknowledged that such volumetric techniques usually better correlate with fracture risk, since they exclude cortical regions like the neural arch and exclusively measure the BMD in the trabecular region, which is known to be metabolically more active and thus more prone to changes in bone mineral density. The use of the presented scout scan-based method as an automatic pre-screening tool, combined with volumetric measures performed in the subsequent CT scan, might be envisioned to provide a fully CT-based osteoporosis screening program.

Moreover, the use of a scout scan for diagnostic purposes could awake concerns regarding the radiation exposure. However, the scout scan is always performed using standard CT protocols, and the developed method thus simply allows a supplementary processing and interpretation of scout scan data that has already been acquired, if the CT scanner used is equipped with an energy-resolving detector. The developed method is fast, and demands only few user interactions, which in the future could be fully automated. The segmentation process used in this study has potential for optimization and

Table 3 BMD measured on two test patients, compared to literature data, since no DXA scan were available. Analysis was repeated four times on the same dataset, for each subject. Indicated errors correspond to standard deviations observed for the four measurements

	L1 (g/cm^2)	L2 (g/cm^2)	L3 (g/cm^2)	L4 (g/cm^2)	Ref. (g/cm^2)*
Young patient (22 years)	0.868 ± 0.023	1.039 ± 0.021	1114 ± 0.020	1.189 ± 0.018	1.04 ± 0.11
Old patient (77 years)	0.725 ± 0.020	0.840 ± 0.013	0.869 ± 0.013	0.791 ± 0.010	0.75 ± 0.08

*Values were extracted from [21] and errors are given as an indication according to the information given in the reference

improvement, for instance with the help of current segmentation technologies used in DXA devices, or of more advanced machine learning techniques [23] which could potentially completely eliminate user interaction. However, no special focus was placed on the refinement and fine tuning of this segmentation method, since the goal of this study was to demonstrate the feasibility of a novel CT scout scan-based method to determine BMD values.

Outlook

Since DXA BMD measurements are evaluated with the help of *T*-scores and *Z*-scores in the clinical routine, one fundamental next step would be to perform a large clinical study, in order to demonstrate that DXA-equivalent *T*- and *Z*-score determination can be performed with the proposed scout scan-based method. This study is also needed in order to evaluate the in vivo test-retest reproducibility of the developed method, as well as its fracture predictability.

Moreover, in some cases, a dual scout scan is acquired (both frontal and lateral). One could also consider this as an improvement strategy of the proposed method, analyzing both the frontal scout scan and the lateral one. The lateral scout scan analysis, transformed in a lateral BMD map, could be used to extend the functionalities of the proposed method and to mimic the functionalities of DXA, for example, by performing vertebral fracture assessment (VFA), hip axis length (HAL) measurement, or body composition assessment.

As this method is not bound to dual-layer spectral detectors, it could also be performed in the future with spectral photon-counting CTs [24–28]. This next generation of energy-resolving detectors would potentially allow to reduce current dose requirements for larger patients as well as to distinguish between oral contrast agent (administered before a scout scan) and calcium [29, 30].

Conclusion

To the best of our knowledge, this is the first study describing the possibility to determine BMD in routinely acquired CT scout scans. The findings were confirmed by extensive phantom experiments and compared to DXA. Moreover, the scout scans from dual-layer CT scanners are systematically acquired using the dual-energy modus, since an advantage of this particular DECT approach is that the spectral data acquisition is always on. If translated into the clinical routine, one possibility would be to determine the BMD fully automatically and only alert the clinician or radiologist when a certain level of BMD is not reached. When considering the high number of CT acquisitions performed worldwide, this could introduce a larger scale opportunistic osteoporosis screening. Essential for this development is the universal availability of CT scanners equipped with spectral detectors (e.g., dual-layer or photon-counting); however, the translation and introduction of such systems are currently in full swing.

Funding We acknowledge support through QRM for providing the ESP phantom, the German Department of Education and Research (BMBF) under grant IMEDO (13GW0072C), the German Research Foundation (DFG - Gottfried Wilhelm Leibniz program), and the DFG within the Research Training Group GRK 2274.

K.B, L.C.F., and R.P. are employees of Philips. The remaining authors have no financial disclosures and had complete, unrestricted access to the study data at all stages of the study.

Compliance with ethical standards

Guarantor The scientific guarantor of this publication is PD Dr. Peter B. Noël.

Conflict of interest The authors of this manuscript declare no relationships with any companies, whose products or services may be related to the subject matter of the article.

Statistics and biometry One of the authors has significant statistical expertise. No complex statistical methods were necessary for this paper.

Informed consent Written informed consent was waived by the Institutional Review Board.

Ethical approval Institutional Review Board approval was obtained.

Methodology
- prospective
- diagnostic study/experimental
- performed at one institution

References

1. Hernlund E, Svedbom A, Ivergård M et al (2013) Osteoporosis in the European Union: medical management, epidemiology and economic burden: a report prepared in collaboration with the International Osteoporosis Foundation (IOF) and the European Federation of Pharmaceutical Industry Associations (EFPIA). Arch Osteoporos 8:136
2. Häussler B, Gothe H, Göl D, Glaeske G, Pientka L, Felsenberg D (2007) Epidemiology, treatment and costs of osteoporosis in Germany - the BoneEVA study. Osteoporos Int 18(1):77–84
3. Glüer CC (2017) 30 years of DXA technology innovations. Bone 104:7–12. https://doi.org/10.1016/j.bone.2017.05.020
4. Curtis JR, Carbone L, Cheng H et al (2008) Longitudinal trends in use of bone mass measurement among older Americans, 1999-2005. J Bone Miner Res 23(7):1061–1067
5. Link TM (2012) Osteoporosis imaging: state of the art and advanced imaging. Radiology 263(1):3–17. https://doi.org/10.1148/radiol.12110462
6. Brett AD, Brown JK (2015) Quantitative computed tomography and opportunistic bone density screening by dual use of computed

tomography scans. J Orthop Translat 3(4):178–184. https://doi.org/10.1016/j.jot.2015.08.006
7. Damilakis J, Adams JE, Guglielmi G, Link TM (2010) Radiation exposure in X-ray-based imaging techniques used in osteoporosis. Eur Radiol 20(11):2707–2714
8. Schwaiger BJ, Kopperdahl DL, Nardo L et al (2017) Vertebral and femoral bone mineral density and bone strength in prostate cancer patients assessed in phantomless PET/CT examinations. Bone 101:62–69. https://doi.org/10.1016/j.bone.2017.04.008
9. Patel AA, Maver DW, Siegel EL (2010) The CT scout exam: a survey of radiation dose, utilization, and opportunity for substantial dose reduction. In: Radiological Society of North America 2010 Scientific Assembly and Annual Meeting. Chicago
10. Bohrer E, Schäfer S, Mäder U, Noël PB, Krombach GA, Fiebich M (2017) Optimizing radiation exposure for CT localizer radiographs. Z Med Phys 27(2):145–158. https://doi.org/10.1016/j.zemedi.2016.09.004
11. Schmidt B, Saltybaeva N, Kolditz D, Kalender WA (2013) Assessment of patient dose from CT localizer radiographs. Med Phys 40(8):084301
12. Alvarez RE, Macovski A (1976) Energy-selective reconstructions in X-ray computerised tomography. Phys Med Biol 21(5):2 Available from: http://stacks.iop.org/0031-9155/21/i=5/a=002?key=crossref.9250d07732e8ba4c630ab8afe8ccd214
13. van Hamersvelt RW, Schilham AMR, Engelke K et al (2017) Accuracy of bone mineral density quantification using dual-layer spectral detector CT: a phantom study. Eur Radiol 27(10):4351–4359
14. Mei K, Schwaiger BJ, Kopp FK et al (2017) Bone mineral density measurements in vertebral specimens and phantoms using dual-layer spectral computed tomography. Sci Rep 7(1):1–10
15. McCollough CH, Leng S, Yu L, Fletcher JG (2015) Dual- and multi-energy CT: principles, technical approaches, and clinical applications. Radiology 276(3):637–653
16. Vlassenbroek A (2011) Dual layer CT. In: Johnson T, Fink C, Schönberg S, Reiser M (eds) Dual Energy CT in Clinical Practice. Medical Radiology. Springer, Berlin, Heidelberg, pp 21–34
17. Ehn S, Sellerer T, Muenzel D et al (2018) Assessment of quantification accuracy and image quality of a full-body dual-layer spectral CT system. J Appl Clin Med Phys 19(1):204–217
18. Carmi R, Naveh G, Altman A (2005) Material separation with dual-layer CT. IEEE Nucl Sci Symp Conf Rec 4:1876–1878
19. Kalender WA, Felsenberg D, Genant HK, Fischer M, Dequeker J, Reeve J (1995) The European Spine Phantom - a tool for standardization and quality control in spinal bone mineral measurements by DXA and QCT. Eur J Radiol 20(2):83–92
20. Yu EW, Thomas BJ, Brown JK, Finkelstein JS (2012) Simulated increases in body fat and errors in bone mineral density measurements by DXA and QCT. J Bone Miner Res 27(1):119–124
21. Wu XP, Liao EY, Huang G, Dai RC, Zhang H (2003) A comparison study of the reference curves of bone mineral density at different skeletal sites in native Chinese, Japanese, and American Caucasian women. Calcif Tissue Int 73(2):122–132
22. Bonnick SL (2008) Monitoring changes in bone density. Womens Health (Lond) 4(1):89–97. https://doi.org/10.2217/17455057.4.1.89
23. Aubert B, Vazquez C, Cresson T, Parent S, De Guise J (2016) Automatic spine and pelvis detection in frontal X-rays using deep neural networks for patch displacement learning. Proc - Int Symp Biomed Imaging; 2016–June:1426–9
24. Pourmorteza A, Symons R, Sandfort V et al (2016) Abdominal imaging with contrast-enhanced photon-counting CT: first human experience. Radiology 279(1):239–245. https://doi.org/10.1148/radiol.2016152601
25. Taguchi K, Iwanczyk JS (2013) Vision 20/20: single photon counting x-ray detectors in medical imaging. Med Phys 40(10):100901. https://doi.org/10.1118/1.4820371
26. Muenzel D, Bar-Ness D, Roessl E et al (2016) Spectral photon-counting CT: initial experience with dual–contrast agent K-edge colonography. Radiology 283(3):723–728
27. Gutjahr R, Halaweish AF, Yu Z et al (2016) Human imaging with photon-counting-based CT at clinical dose levels: contrast-to-noise ratio and cadaver studies. Invest Radiol 51(7):421–429
28. Willemink MJ, Persson M, Pourmorteza A, Pelc NJ, Fleischmann D (2018) Photon-counting CT: technical principles and clinical prospects. Radiology 172656. https://doi.org/10.1148/radiol.2018172656
29. Dangelmaier J, Bar-Ness D, Daerr H et al (2018) Experimental feasibility of spectral photon-counting computed tomography with two contrast agents for the detection of endoleaks following endovascular aortic repair. Eur Radiol 28(8):3318–3325
30. Cormode DP, Si-Mohamed S, Bar-Ness D et al (2017) Multicolor spectral photon-counting computed tomography: in vivo dual contrast imaging with a high count rate scanner. Sci Rep 7(1):1–11